Simulations of impulsive laser scattering of biological protein assemblies: Application to M13 bacteriophage

Eric C. Dykeman,* Daryn Benson, K.-T. Tsen, and Otto F. Sankey†
Department of Physics, Arizona State University, Tempe, Arizona 85287, USA
(Received 11 February 2009; revised manuscript received 17 July 2009; published 7 October 2009)

We develop a theoretical framework, based on a bond-polarizability model, for simulating the impulsive force experienced on a protein or an assembly of proteins from a pulsed light source by coupling the laser electric field to an atomic distortion. The mechanism is impulsive stimulated Raman scattering (ISRS) where mechanical distortions produce variation in the electronic polarization through atomic displacements similar to vibrational Raman scattering. The magnitude of the impulsive force is determined from the empirical two-body bond-polarizability model and the intensity of the incident light. We apply the method to the M13 bacteriophage protein capsid system by performing several classical molecular-dynamics simulations that include the additional impulsive laser scattering force at various light intensities and pulse widths. The results of the molecular-dynamics simulations are then qualitatively interpreted with a simple harmonic oscillator model driven by ISRS. The intensity of light required to produce damage to the capsid in the simulations was found to be far higher than what was found in recent pulsed laser scattering experiments of M13 phage, suggesting that the observed inactivation of viruses with ultrashort laser pulses involves processes and/or mechanisms not taken into account in the present simulations.

DOI: 10.1103/PhysRevE.80.041909 PACS number(s): 87.15.La, 87.64.kp, 87.19.xd, 87.50.ct

I. INTRODUCTION

Raman laser scattering is an ubiquitous tool to nondestructively study the vibrational modes of condensed systems. The electric field of the light interacts with the charge density of system which is modulated by a vibration of the atoms. Raman scattering produces scattered light that is shifted by the frequency ω of the vibration. Monitoring these shifts gives information about the microscopic state of the observed system. Raman scattering with temporally ultrashort pulses gives rise to an additional effect. It can be used to selectively excite large amplitude vibrations producing a unique kind of athermal excitation of the material. In this paper, we develop a theory to model this unique effect, called impulsive stimulated Raman scattering (ISRS), in biological materials, specifically assemblies of proteins.

As an application, we apply the theoretical model to determine the light intensity necessary to produce very large amplitude excursions from equilibrium for an M13 bacteriophage capsid made exclusively of proteins. A viral capsid is the outer protein shell that protects the genomic material enclosed inside. We specifically explore the parameters necessary to produce a large amplitude excursion and to produce damage which compromises the integrity of the capsid.

An example of the need for a theoretical methodology and simulation of ISRS in biological systems are the results of ultrashort laser studies on a variety of viral particles. Tsen and colleagues [1–5] performed several experiments with M13 bacteriophages, and other viral particles, in solution. Using conditions suggesting ISRS with near-infrared and visible light, they have been able to inactivate many viruses with different morphologies including M13, TMV, HPV, and HIV. However, it is not known if ISRS is the mechanism involved in the inactivation or if other processes enable the inactivation. The present work shows that significant damage from a single laser pulse occurs only for laser intensities far higher than those used in the experiments, suggesting that processes or mechanisms not included in the simulations are operative.

Basic light scattering experiments (not ISRS) to determine the vibrational modes of a capsid have produced mixed results. Stephanidis *et al.* [6] performed Brillouin scattering on satellite tobacco mosaic viruses and did not detect virus particle mechanical modes. The reason for this is not clear. Tsen *et al.* [7] performed Raman scattering experiments on M13 and determined a clear peak at low frequency. This work was in solution and the intensity of the "extra" Raman peak at low frequency was proportional to the viral concentration. This provides evidence that dampening does not destroy viral mechanical modes.

These are the first simulations of ISRS for a biological protein system, such as a virus, ever reported. In these initial molecular-dynamics (MD) simulations we seek primarily a qualitative understanding of how ISRS may affect the stability of a protein assembly. Our focus will be on global motions of the protein system since these are most likely to disrupt the viral capsids. Global motions are expected to be of low frequency (say 100 GHz) due to the large effective mass of a collective displacement of many atoms. We search for effects produced by pulsing the laser where the duration of the pulse is comparable to the period for global oscillatory motion of the capsid. For these initial simulations we choose not to explicitly include the effects of solvent which surely are important but complicate a simple qualitative analysis. The effects of the solvent on the energetics of the capsid are at least approximately included in the explicit solvent generalized Born model used here (described below). However,

*Present address: Department of Biology, University of York, York YO10 5DD, United Kingdom.
†Corresponding author. Email: otto.sankey@asu.edu

the important effect of solvent dampening is lacking in this model. Future work will examine the more complicated picture where explicit solvent can dampen the mechanical oscillations that have been excited via ISRS.

The ISRS mechanism is a scattering phenomena and not an absorption process. The use of molecular dynamics to study direct absorption effects of electromagnetic field interactions with proteins has been attempted previously. English and Mooney [8] studied the denaturation of hen egg white lysozyme in electromagnetic fields using molecular dynamics. In their work, they included the Lorenz force in the molecular-dynamics simulation which resulted from light of constant intensity. This produces a driving force on the atoms which is harmonic and at the frequency of the incident light. For large global atomic motions to properly follow the electric field of the incident light, the frequency of the light must be orders of magnitude lower in frequency than that of visible light. Our approach is fundamentally different. For ISRS, the frequency of the light can be in the visible, but it is scattered not absorbed. Essentially, the heavy nuclei are unable to follow the rapid oscillations of the electric field while the less massive electrons are able to instantaneously follow the electric field oscillations and induce a near instantaneous polarization. The mechanism in which the rapid electron motion produces a force on the nuclear degrees of freedom is through the induced electron polarization, which we model as an additional energy and force within shared bonds. The effect of the light scattering does not lead to a harmonic force on the atoms, but rather couples to the average intensity, which is dc and is modulated by the pulse shape of the incident laser light. For ultrashort pulses (e.g., on the order of picoseconds), the atoms experience a brief (impulsive) force. Thus the impulsive stimulated Raman scattering technique introduces an average electromagnetic intensity which has a Gaussian profile of short duration τ_L.

An ultrashort pulse of visible light is not the only means to excite mechanical distortions. The direct absorption of electromagnetic energy at a vibrational frequency of oscillation is another possibility. For large assemblies, this would require frequencies in the GHz to THz range. These frequencies are in the microwave to t-ray range. Frequencies in this region are highly absorbed by water, and have heating effects on the environment. Visible light is transparent in water and is better capable of penetrating protein solutions.

The material in this paper is broken up into three main divisions as follows. In the next section, we describe the theoretical model used to predict the force on a polarizable bond that results from impulsive stimulated Raman scattering by an incident electromagnetic field. The theory extends the work of Nelson *et al.* [9] to large biological systems and becomes semiquantitative by introducing an empirical bond-polarizability (BP) model to predict the polarization field. The polarization is used to obtain the potential energy of the polarizable bond in the electric field and a relatively simple formula for the additional ISRS force within a bond results. Next, we apply this and discuss the molecular-dynamics simulations which use a periodic segment of the M13 bacteriophage capsid with the additional impulsive force of light along with the traditional molecular-dynamics forces. Finally the results of the computer simulations are presented followed by a qualitative analysis of the ISRS effect on the M13 capsid in terms of the physics of a simple driven harmonic oscillator.

II. THEORY

Consider a light scattering process where the electromagnetic field from the light has short time duration τ_L. The nimble electrons react adiabatically to the electric field and produce a polarization field. The polarization radiates and, in effect, scatters the incident light. The polarizability of the protein system is modulated by the motion of the nuclei of its constituent atoms, to produce a component of the scattered light that is downshifted (Stokes) or upshifted (anti-Stokes) by the protein vibrational frequencies. This is the basic Raman scattering process from continuous wave experiments. The ISRS mechanism activates vibrational modes of various frequencies differently depending on the time τ_L of the incident pulse. We seek to derive a formula that gives the resulting force exerted on a polarizable bond from the *pulsed* light source which can be added to the internal forces within an MD protocol.

A description of the polarization field within the protein assembly is necessary in order to determine the coupling of the capsid to the external electric field. In general, this is extraordinarily difficult to obtain since the polarizability of a molecule depends on the electronic wave functions and electron density of the entire molecule. To advance our study, a simplified empirical bond-polarizability model [10] is used. In this model, the total polarization is a sum of polarizations of each of its bonds. Such models have been successfully used to predict the Raman intensity profiles of organics [11] and C_{60} and C_{70} fullerene [12,13], and have also recently been used to predict relative Raman intensity profiles of viral capsids in solution [14,15].

Using the bond-polarizability model, the force on a general bond can be derived in terms of four parameters (described below). This formula for the force can then be used in a molecular-dynamics simulation, effectively incorporating the coupling of light to the protein system.

III. BOND POLARIZABILITY MODEL

We consider the electronic polarizability of a protein complex as being composed of a sum of polarizabilities of individual bonds within the complex. The polarizability is assumed to be constant with no frequency dependence of the incident light. The model is appropriate for the nonresonant Raman effect, but not the resonant Raman effect which occurs when the frequency of light is near an electronic transition. In our model, the light must have frequencies far below any electronic absorption thresholds. Additionally a bond is considered to exist between atoms of the protein which are coupled by springs in the force field parametrization—the van der Waals "bonds" or hydrogen bonds are not considered bonds in the sense of adding a significant bond polarizability.

In the BP model, the polarizability of a single bond is described by four parameters—two are the parallel and perpendicular polarizabilities, $\alpha'_{\parallel}$ and $\alpha'_{\perp}$, of the bond at its

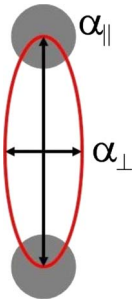

FIG. 1. (Color online) A diagram of the bond-polarizability ellipse. The polarizability tensor of a bond has components that are parallel ($\alpha_{\|}$) and perpendicular ($\alpha_{\perp}$) to the bond. The parameters $\alpha_{\|}$ and $\alpha_{\perp}$ describe the polarizability of the bond at its equilibrium configuration while $\alpha'_{\|}$ and $\alpha'_{\perp}$ are the derivatives of these parameters with respect to bond length (i.e., $\frac{\partial}{\partial d}$).

equilibrium bond length d, while the other two are the polarizability derivatives $\alpha'_{\|}$ and $\alpha'_{\perp}$ ($\alpha' \equiv \frac{\partial \alpha}{\partial d}$) that describe changes in the parallel and perpendicular polarizability parameters due to bond stretching. This gives a description of the polarization field of a bond that is often referred to as the polarization ellipse. A simple diagram of the polarization ellipse is shown in Fig. 1. Proteins are composed of a variety of single and double bonds between H, C, N, O, and S. For basic qualitative purposes, we model all the bonds in the protein complex as having one set of polarizability parameters. Future work will incorporate a more intricate model which produces parameters for each atom pair and the hybridization (e.g., sp^2 or sp^3) of the bond. For this work we use parameters for all bonds determined by a representative single bond, the carbon-carbon bond. There have been several parameterizations of this bond, much of it centered on the fullerenes. Three parametrizations for C-C bonds are shown in Table I and one can gain a sense of the variation in the fits of these values. The magnitude of the polarizability is of order the volume of the bond. The force depends on only three parameters of the polarizability and its derivatives [$\alpha'_{\|}$, $\alpha'_{\perp}$, and the combination $(\alpha_{\perp}-\alpha_{\|})/d$] and only these parameters are listed. In this work we use the values in the first column from Bermejo *et al.* [11], as these were fit to simple organic hydrocarbons, which is closer to the case at hand. The values of Snoke *et al.* [13] and Guha *et al.* [12] were fit specifically to C_{60}.

TABLE I. Three different parametrization of the bond polarizability of the C-C single bond. The values used in the simulation of this paper are those of the first column from Bermejo *et al.* [11], which fit simple organic molecules. The Snoke and Guha fits were specifically for C_{60}. The value of d used so that different parametrizations can be represented in one system is 1.44 Å, which is between the single and double bonds of C_{60}. The values shown are in Gaussian units where polarizabilities have units of volume. Converting to MKS is accomplished by multiplying the values in the table by $4\pi\epsilon_0$.

	Bermejo *et al.* [11]	Snoke *et al.* [13]	Guha *et al.* [12]
$(\alpha_{\|}-\alpha_{\perp})/d$	1.04 Å^2	2.48 Å^2	0.89 Å^2
$\alpha'_{\|}$	2.89 Å^2	3.66 Å^2	2.30 Å^2
$\alpha'_{\perp}$	0.33 Å^2	~0 Å^2	0 Å^2

As the protein system vibrates, a bond in the structure between atoms i and j with coordinates $\vec{r}_i$ and $\vec{r}_j$ will have variable bond length $d=|\vec{r}_i-\vec{r}_j|$ and variable orientation, which can be described by the unit vector $\hat{d}$. The 3×3 polarizability tensor of the bond ($\overleftrightarrow{\alpha}$) can be written in terms of the bond projector operator [13,14] $\hat{P}=|\hat{d}\rangle\langle\hat{d}|$, as

$$\overleftrightarrow{\alpha} = \alpha_{\|}\hat{P} + \alpha_{\perp}(\hat{I}-\hat{P}), \tag{1}$$

where $\hat{I}$ is the 3×3 identity matrix. As the electric field is incident on the bond, a time-dependent polarization field $\vec{p}(t)$ is created,

$$\vec{p}(t) = \overleftrightarrow{\alpha}\cdot\vec{E}(t). \tag{2}$$

The resulting potential energy of the bond takes the form

$$U(t) = -\frac{1}{2}\vec{p}\cdot\vec{E},$$

$$U(t) = -\frac{1}{2}\vec{E}\cdot\overleftrightarrow{\alpha}\cdot\vec{E}. \tag{3}$$

The factor of $\frac{1}{2}$ comes from the build up of polarization with E field, much as the same factor that occurs in the charging energy of a capacitor.

IV. IMPULSIVE RAMAN FORCE ON A BOND

The impulsive force on a single bond that results from an inelastic scattering process follows from the potential energy of the bond in an electric field [9]. For impulsive stimulated Raman scattering, the electric field is a Gaussian wave packet with pulse width τ_L and frequency ω_L,

$$\vec{E}(t) = \vec{E}_0 e^{-t^2/2\tau_L^2}\cos(\omega_L t), \tag{4}$$

where the peak electric field amplitude has been chosen to occur at $t=0$. The spatial dependence of the electric field has been ignored since the dimensions of a bond or protein are much smaller than the wavelength of light used in ISRS experiments (500–800 nm) [2,3]. Combining Eq. (4) with Eq. (3), one obtains

$$U(t) = -\frac{1}{2}\vec{E}_0\cdot\overleftrightarrow{\alpha}\cdot\vec{E}_0 e^{-t^2/\tau_L^2}\cos^2(\omega_L t). \tag{5}$$

The period of the bond oscillations ($T_b>10$ fs) are much longer than that of visible light ($T_L\sim2$ fs for 600 nm light); thus the potential energy contribution from a single bond [Eq. (5)] can be time averaged over one period of the electric field to give

$$U(t) = -\frac{1}{4}\vec{E}_0\cdot\overleftrightarrow{\alpha}\cdot\vec{E}_0 e^{-t^2/\tau_L^2}. \tag{6}$$

Since a protein system consists of a network of bonds, the total potential energy is a sum of Eq. (6) over all bonds. The

αth component (x, y, or z) of the force of light on atom i is obtained from the derivative of the total potential energy of the bond network with respect to atomic position $r_{i\alpha}$,

$$\vec{F}^L_{i\alpha}(t) = \frac{1}{4}\sum_{\text{bonds}} \vec{E}_0 \cdot \frac{\partial \vec{\vec{\alpha}}_{\text{bond}}}{\partial r_{i\alpha}} \cdot \vec{E}_0 e^{-t^2/\tau_L^2}. \tag{7}$$

The derivative of $\vec{\vec{\alpha}}_{\text{bond}}$ with respect to $r_{i\alpha}$ is nonzero only if the bond contains atom i. Examining the contribution to atom i from one bond of length d, the derivative of the polarizability tensor $\vec{\vec{\alpha}}$ takes the form

$$\frac{\partial \vec{\vec{\alpha}}_{bond}}{\partial r_{i\alpha}} = \frac{\partial d}{\partial r_{i\alpha}}[\alpha'_{\parallel}\hat{P} + \alpha'_{\perp}(\hat{I} - \hat{P})] + (\alpha_{\parallel} - \alpha_{\perp})\frac{\partial \hat{P}}{\partial r_{i\alpha}}. \tag{8}$$

Small bond oscillations have been assumed in Eq. (8) so that the four polarizability constants can be evaluated at the equilibrium bond length. The projection operator $\hat{P}$ has components given by $\hat{P}_{\beta\gamma} = \hat{d}_\beta \hat{d}_\gamma$, where $\hat{d}_\beta$ is the β component of the bond unit vector. The derivatives of the bond unit vector with atomic position are

$$\frac{\partial \hat{d}_\beta}{\partial r_{i\alpha}} = -\frac{1}{d}\frac{\partial d}{\partial r_{i\alpha}}\hat{d}_\beta + \frac{\delta_{\alpha\beta}}{d}. \tag{9}$$

Substituting Eqs. (9) and (8) into Eq. (7) followed by some algebra results in

$$F^L_{i\alpha}(t) = [f_d \hat{d}_\alpha + f_E \hat{E}_\alpha]\frac{|E_0|^2}{4} e^{-t^2/\tau_L^2}. \tag{10}$$

The force on the atom from impulsive light scattering has two components—one component is along the direction of the bond, and the second is along the direction of the electric field. The factors f_d and f_E are

$$f_d = (\hat{E}_0 \cdot \hat{d})^2\left[\alpha'_{\parallel} - \alpha'_{\perp} - \frac{2(\alpha_{\parallel} - \alpha_{\perp})}{d}\right] + \alpha'_{\perp},$$

$$f_E = 2\frac{(\alpha_{\parallel} - \alpha_{\perp})}{d}(\hat{E}_0 \cdot \hat{d}). \tag{11}$$

Equation (10) describes the force contribution to atom i from the light scattering of a single bond containing atom i. These two equations [Eqs. (10) and (11)] provide the additional force necessary for molecular-dynamics simulations of impulsive stimulated Raman scattering of protein systems. We note that Eq. (10) is a time average force where the rapid oscillations of the intensity [$\sim\cos^2(\omega_L t)$] are replaced by the dc component of 1/2. Again, this approximation is justified from the short period of visible light when compared to that of a typical bond.

The force depends on the three parameters $\alpha'_{\parallel}$, $\alpha'_{\perp}$, and $(\alpha_{\perp} - \alpha_{\parallel})/d$, on the laser light electric field strength and on the width of the laser pulse τ_L. The electric field strength is obtained from the intensity I_0 of the laser light, $I_0 = \frac{1}{2}\epsilon_0 c|E_0|^2$ (neglecting dielectric effects). For a given set of polarizability parameters (Table I) the additional variables necessary for an MD simulation are the external laser intensity I_0 and pulse time τ_L. We present simulations varying these two parameters in the results section.

V. ISRS OF THE DRIVEN HARMONIC OSCILLATOR

There is rich content in the analysis of ISRS in terms of normal modes. Normal mode analysis assumes a harmonic potential and small displacements $\vec{u}$ from equilibrium. Our conceptual analysis of the molecular-dynamics simulations of impulsive light scattering from a large protein assembly such as an M13 capsid uses the harmonic approximation as a foundation to break the problem up into many (of order $\sim$100 000) independent driven harmonic oscillations. In this description, the full motion is the sum of all independent normal mode excursions. Of course, the MD simulation itself is not dependent on such an approximation, but a simple driven harmonic oscillator analysis forms a useful foundation to understand the complex MD results.

In the harmonic approximation, Newton's equation of motion for $3N$ displacements of atom i in the direction α around equilibrium is

$$M_i \ddot{u}_{i\alpha} + \sum_{j\beta} \phi_{i\alpha,j\beta} u_{j\beta} = 0, \tag{12}$$

where $\phi_{i\alpha,j\beta}$ is the force constant matrix. The normal mode ν oscillates at frequency ω_ν and the displacement pattern forms a generalized vector $|\vec{\eta}_\nu\rangle$ of length $3N$. The normal modes satisfy the eigenvalue equation

$$-\omega_\nu^2 \vec{\vec{M}}|\vec{\eta}_\nu\rangle + \vec{\vec{\phi}}|\vec{\eta}_\nu\rangle = 0, \tag{13}$$

where $\vec{\vec{M}}$ is the diagonal mass matrix with components $M_{i\alpha,j\beta} = m_i \delta_{ij}\delta_{\alpha\beta}$. This equation can be transformed into a dynamical matrix with mass weighted coordinates $|\vec{\eta}_\nu\rangle = \vec{\vec{M}}^{-1/2}|\hat{e}_\nu\rangle$,

$$-\omega_\nu^2|\hat{e}_\nu\rangle + \vec{\vec{D}}|\hat{e}_\nu\rangle = 0, \tag{14}$$

where $D_{i\alpha,j\beta} = \phi_{i\alpha,j\beta}/\sqrt{m_i m_j}$ and the eigenvectors $|\hat{e}\rangle$ are orthonormal, $\langle \hat{e}_\nu|\hat{e}_{\nu'}\rangle = \delta_{\nu\nu'}$, while the displacements patterns themselves satisfy $\langle \vec{\eta}_\nu|\vec{\vec{M}}|\vec{\eta}_{\nu'}\rangle = \delta_{\nu\nu'}$.

A general displacement can be expanded into normal modes via

$$|\vec{u}(t)\rangle = \sum_\nu Q_\nu(t)|\vec{\eta}_\nu\rangle. \tag{15}$$

Substituting Eq. (15) into Eq. (12) and applying $\langle \eta_\nu|$ we obtain the equation of motion for the normal coordinate Q_ν,

$$\ddot{Q}_\nu + \omega_\nu^2 Q_\nu = 0, \tag{16}$$

which exhibits simple harmonic motion of frequency ω_ν.

Next we introduce the force from the intensity of the laser. An additional force exists on each atom, $\vec{F}^L_i$, and Newton's equation of motion [Eq. (12)] becomes

$$M_i \ddot{u}_{i,\alpha} + \sum_{j,\beta} \phi_{i\alpha,j\beta} u_{j\beta} = F^L_{i\alpha}. \tag{17}$$

The force vector in configuration space comes from the gradient of a potential energy V; $|\vec{F}^L\rangle = \Sigma_{i\alpha} F^L_{i\alpha}\hat{x}_\alpha = \Sigma_{i\alpha} -\frac{\partial V}{\partial u_{i\alpha}}\hat{x}_\alpha$. This force is the additional force of light to add to an MD simulation. The force on a specific mode Q_ν is easily derived using $F_{Q_\nu} = -\frac{\partial V}{\partial Q_\nu}$, which results in

$$F_{Q_\nu} = \langle \vec{\eta}_\nu | \vec{F}^L \rangle. \tag{18}$$

The force in real space $|\vec{F}^L\rangle$ due to the laser intensity was determined in the previous section. The important point here is that, when viewed in the space of normal modes, the force on the normal mode is given by the scalar product of the displacement pattern for that mode and the force on each of the atoms within that mode. The equation of motion for each normal mode is then

$$\ddot{Q}_\nu + \omega_\nu^2 Q_\nu = F_{Q_\nu}, \tag{19}$$

which is that of a driven harmonic oscillator.

The form of the force for a Gaussian laser pulse is $F_{Q_\nu} = g(t)F_0$, where $g(t) = e^{-t^2/\tau_L^2}$ and F_0 is the amplitude of the force which [via Eq. (10)] is proportional to the light intensity I_0. The response for a driven harmonic oscillator can be determined from the Green's function, and for times long after the pulse ($t \gg \tau_L$), the solution is

$$Q_\nu(t) = \sqrt{\pi}\left(\frac{\tau_L}{\omega_\nu}\right) F_0 e^{-\omega^2 \tau_L^2/4} \sin(\omega_\nu t), \tag{20}$$

where the amplitude of the oscillation (neglecting damping) is $Q_{0,\nu} = \sqrt{\pi}(\frac{\tau_L}{\omega_\nu})F_0 e^{-\omega^2\tau_L^2/4}$. To excite a specific mode of frequency ω_ν, the largest amplitude ($dQ_{0,\nu}/d\tau_L = 0$) occurs when the laser pulse time is equal to $\omega_\nu \tau_L = \sqrt{2}$. Using $\omega_\nu = 2\pi/T$, this becomes $\tau_L = 0.225T$ or near $\tau_L = \frac{1}{4}T$, which is analogous to pushing a child on a swing.

A useful quantity to compute is the total energy in all the modes after the light pulse has left and the driving force is zero. This will provide a description of how well the ISRS pulse transfers energy to the target during the scattering process. Using Eq. (20), the energy of a mode is given by

$$E_\nu = \frac{1}{2} Max\{\dot{Q}_\nu^2(t)\} = \frac{1}{2}\omega_\nu^2 Q_{0,\nu}^2 = \frac{\pi}{2}\tau_L^2 F_0^2 e^{-\omega^2\tau_L^2/2}. \tag{21}$$

For a single acoustic branch in d dimensions ($d = 1$, 2, or 3), the density of states is given by $D(\omega) = D \times \omega^{d-1}$. Although the density of states of a large protein complex will not follow anything so simple, it serves as a useful rough estimate for developing an intuitive feel for the total energy delivered (TED) to the target. We will use the density of states in three dimensions, $D(\omega) = D\omega^2$, as a qualitative density of states for the target (in our example, a virus capsid)

Using Eq. (21) for the energy of mode ν and assuming an ω^2 dependence of the density of states, we obtain the continuous energy absorption density (EAD) as a function of ω,

$$D_{\mathrm{EAD}}(\omega) = C I_0^2 \omega^2 \tau_L^2 e^{-\omega^2\tau_L^2/2}, \tag{22}$$

where C is a factor that is proportional to $\langle \vec{\eta}_\nu | \vec{F}^L \rangle^2$. Although C will have some ω dependence, we assume for simplicity that it is weak when compared with the Gaussian dependence from the light pulse. A plot of the EAD can be seen in Fig. 2 for various pulse widths of the laser τ_L. The EAD plot shows a key feature of the ISRS scattering process—selectivity. Long pulse widths are strongly coupled to the low frequency modes while shorter pulse widths are strongly coupled to the high frequency modes. The maximum of the EAD occurs at $\omega\tau_L = \sqrt{2}$ or when the pulse width of the light is approximately one quarter the period of the system's vibration.

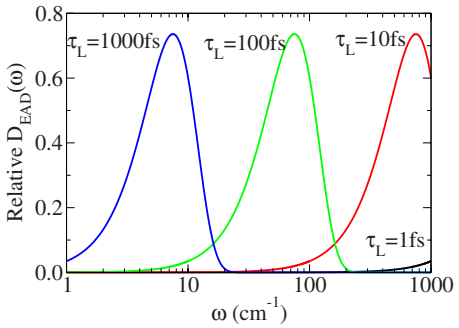

FIG. 2. (Color online) The relative energy absorption density, $D_{\mathrm{EAD}}(\omega)$, for different Gaussian pulse durations τ_L. The EAD is a qualitative measure that shows the degree of excitation of modes of various frequencies. The simple model assumes harmonic restoring forces, a Raman cross section that is independent of frequency, and a density of vibrational states proportional to ω^2. The EAD clearly shows that only certain regions of the spectrum become excited by the pulse duration τ_L of the laser pulse.

The total energy delivered to the target can be calculated from the EAD by integrating over all frequencies,

$$E_{\mathrm{TED}} = \int_0^\infty D_{\mathrm{EAD}}(\omega)d\omega = C I_0^2 \tau_L^2 \int_0^\infty \omega^{d-1} e^{-\omega^2\tau_L^2/2} d\omega. \tag{23}$$

For three dimensions $d = 3$, we obtain $E_{\mathrm{TED}} \propto I_0^2/\tau_L$. This is of course just a rough qualitative estimate, but it shows surprising features. First, the energy delivered to the target increases quadratically with laser intensity. Second, and even more unexpected, shorter pulses deposit more energy than longer pulses. These two features contrast sharply with the energy deposited due to absorption which deposits energy proportional to $I_0\tau_L$. However, one must not interpret this result too literally since the dependence on density of states is qualitative—the true density of states will have many peaks and distinctive features. Finally, we note in passing that energy deposited due to two-phonon absorption also is expected to scale as I_0^2. One must be careful with conclusions comparing two-photon absorption with ISRS. Two photon absorption will scale overall as $I_0^2\tau_L$, while ISRS has a more uncertain τ_L dependence even scaling in our approximation as I_0^2/τ_L.

VI. METHODS

A. Structure of M13 bacteriophage

The example system we use for the simulation of impulsive Raman scattering from a protein assembly is the M13 bacteriophage capsid. The M13 bacteriophage is a long filamentous tube composed of many α-helix building blocks, each helix containing 50 amino acids. Figure 3(a) shows a diagram of a single α-helix building block which is approximately 7 nm in length. The coordinates of the α-helix build-

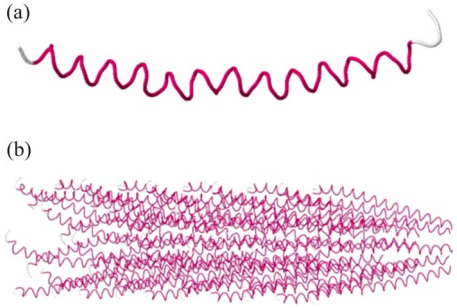

FIG. 3. (Color online) Structure of the M13 bacteriophage tubular capsid. (a) Structure of a single α-helix building block used to construct the full capsid. The α-helix building block contains 50 amino acids and is roughly 7 nm in length. (b) A unit cell periodic segment of the M13 bacteriophage capsid constructed with 50 of the α-helix building blocks wrapped in a helical fashion. The unit cell is periodically repeated along the tube direction. The length of the unit cell is approximately 16 nm.

ing block shown in Fig. 3(a) were determined by x-ray crystallography [16] and were obtained from the protein data bank (PDB code 2C0W).

The α-helix building blocks assemble in a helical fashion on the surface of a cylinder to form a long hollow tube, which houses and protects the viruses' genome consisting of circular single stranded DNA. The total length of the M13 capsid has some variation, but is usually around 800 nm. Figure 3(b) shows a section of the M13 capsid built from 50 of the α-helix building blocks. The structure was built by applying the helical operators provided in the PDB file. The resulting structure in Fig. 3(b) is approximately 16 nm in length and is aligned along the z axis (tube axis).

The full capsid structure is periodic along the tube axis, and we treat it as an infinitely long tube. Our simulations use periodic boundary conditions (PBCs) and we treat one unit cell (50 protein units) with all degrees of freedom. The total number of atoms in the unit cell is $N=37\,050$, which gives a total of $3N=111\,150$ degrees of freedom. Care must be taken since PBCs essentially ignore the effects that the laser pulse has on the ends of the capsid. Raman scattering has a quasimomentum conservation law [17] and since visible light has a relatively long wavelength (≈ 600 nm) this gives the usual approximation for Raman scattering that excited modes have $k \approx 0$. Using periodic boundary conditions for the molecular-dynamics simulation is equivalent to $k \approx 0$.

B. Computational methodology

In this section we describe the computational methods used in the MD simulations. Of interest is the TED to the target from the impulsive light scattering. We use constant energy constant volume (microcanonical ensemble) molecular-dynamics simulations to probe this question. By "constant energy" we mean that there is no energy redistribution due to a heat bath, but energy from the electromagnetic wave scattering can flow into (or out of) the molecular system by the ISRS external forces [Eq. (10)].

A periodic segment of our example target, an M13 bacteriophage capsid, is shown in Fig. 3(b), which was first energetically minimized using the AMBER 94 [18] force field. Explicit water was not used in the calculation. To account for energetic interactions of the capsid with water, the implicit generalized Born solvation model [19–21] was used for the Coulomb interactions. The generalized Born model uses a dielectric screening methodology allowing for the Coulomb sum to be truncated. Thus, no Ewald summation was used although periodicity exists. A 10 Å cutoff was used in the simulations. As a result, the Coulomb sum only extends slightly into neighboring cells. The lack of explicit water will of course neglect damping that occurs as a result of solvent pressure on the capsid. The goal of this paper though is to examine the basic physics of impulsive stimulated Raman scattering of a protein assembly and gain a qualitative understanding that is necessary for future work. Explicit water is an important consideration to be incorporated in future work.

After the capsid was energetically minimized, several molecular-dynamics simulations using different pulse widths (τ_L) and intensities (I_0) of light were performed using the additional force derived above [Eqs. (10) and (11)]. All MD simulations which have the additional force from ISRS set the initial thermal equilibrium temperature of the capsid to $T \approx 0$ K. The light pulse duration was varied from 10 fs to 10 ps and the light intensities were varied from 0.7 PW/cm^2 to 2 PW/cm^2. The initial system time was set to at least $t_0 = -2\tau_L$ to allow for one single pulse of light to completely interact with the capsid. The total length of the simulations varied, depending on the pulse width, but was around 1 ns in total length. Since the lowest frequency modes of the M13 bacteriophage capsid are around 1 cm^{-1} [22] (corresponding to a period of 33 ps), the 1 ns MD simulations will allow enough time for several vibrational cycles of the capsid. If the capsid is damaged, it is likely that the damage occurs in

TABLE II. Total energy delivered to an M13 capsid from a classical molecular-dynamics simulation that has incorporated an ISRS force. The table shows various energy values for different pulse widths (τ_L) and intensities of the light (I_0). An asterisk next to the value in the table indicates that the capsid was damaged by the end of the simulation. Two asterisks indicate that the capsid protein units became completely separated by end of the simulation. The intensities are given in PW/cm^2, pulse widths in ps, and the energies in keV.

	$I=0.7$	$I=0.8$	$I=0.9$	$I=1.0$	$I=1.5$	$I=2.0$
$\tau_L=0.01$	2.698*	3.517*	4.447*	5.489*	12.470**	22.152**
$\tau_L=0.10$	0.656*	0.793*	0.918*	1.045*	1.733**	2.368**
$\tau_L=1.00$	0.488*	0.537*	0.587*	0.617*	0.859**	1.068**
$\tau_L=10.0$	0.344*	0.406*	0.429**	0.465**	0.579**	0.656**

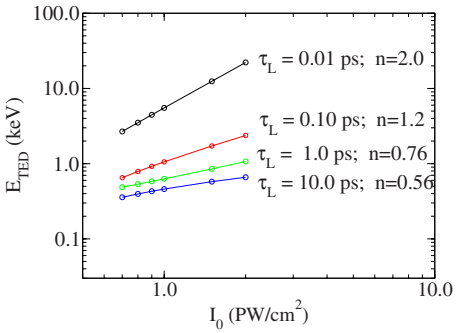

FIG. 4. (Color online) The dependence on the total energy deposited (TED) as a function of Intensity on a log-log plot from MD simulations. The TED fits a power law, $E_{\mathrm{TED}}=AI_0^n$, where n varies from 0.56 to 2.0 for different pulse durations τ_L.

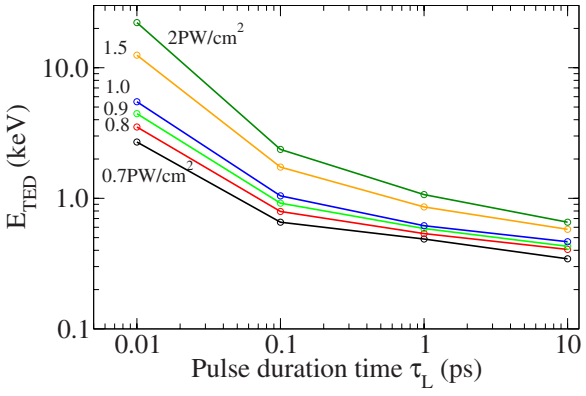

FIG. 5. (Color online) The dependence on the total energy deposited (TED) as a function of the laser pulse duration τ_L on a log-log plot for different values of the incident energy flux from MD simulations.

the first few vibrational cycles. This becomes even more likely in explicit water where the dampening effects will diminish the vibrational energy within a few cycles.

VII. RESULTS

A total of 24 MD simulations of roughly 1 ns in length were performed in the intensity range of 0.7 PW/cm^2 to 2 PW/cm^2 and the pulse width range of 10 fs to 10 ps. For each MD simulation, the total energy delivered to the capsid was calculated from the MD energy data via the total energy deposited, $E_{\mathrm{TED}}=E_f-E_i$, where E_i is the total (kinetic plus potential) initial energy of the M13 capsid and E_f is the "final" internal energy of the capsid after the light pulse has passed through. Table II lists the results for the various pulse widths and intensities of light. An asterisk next to the TED values in the table indicates that the viral capsid exhibited damage in the form of a small pore on the capsid surface by the end of the MD simulation. Two asterisks indicate that the capsid was completely broken apart (i.e., the individual α-helix building blocks became separated) by the end of the simulation. In general, the time scale for the capsid to be broken apart is around 20–30 ps, which is consistent with 1 vibrational cycle of a low frequency (1 cm^{-1}) mode. It is of interest to note that more energy deposited does not necessarily break apart the capsid. This suggests, due to the selectivity of ISRS, that it is important into which mechanical modes the energy is deposited.

A plot of the TED computed from the MD simulations is shown in Fig. 4 for different pulse durations τ_L. A harmonic analysis predicts that $E_{\mathrm{TED}}\sim I_0^2$. Fitting the data to a power law dependence ($E_{\mathrm{TED}}=AI_0^n$) shows that the power $n=2$ dependence is satisfied for a very short pulse time ($\tau_L=0.01$ ps) but drops down significantly from 2 for longer laser pulse times (e.g., $n=0.56$ for $\tau_L=10$ ps). Presumably this occurs because shorter pulses excite harmonic (within the force field model) spring like bond-stretching modes, but longer pulses excite anharmonic global modes involving interactions between residues or between proteins.

Figure 5 shows the dependence on the TED as a function of the laser pulse duration (τ_L) on a log-log plot for different values of the incident energy flux. The data displays a clear tendency for the TED to decrease as the pulse duration is increased, confirming the general prediction from a simple harmonic analysis. However the TED is clearly not simply inversely proportional to τ_L. Since low frequency modes are stimulated more strongly for long τ_L than high frequency modes, this likely reflects a more complicated density of states of the capsid and/or a different coupling of the impulsive light force to the various vibrational modes of the capsid.

An example of a capsid that has been severely damage d is illustrated in Figs. 6(a)–6(d). The intensity of light for this simulation was 1.5 PW/cm^2 and the pulse width was $\tau_L=1$ ps. Figure 6 shows trajectory snapshots of the capsid structure over roughly a single vibrational cycle (~20 ps) of the 1 ns MD simulation. At later times, the capsid continues its outward expansion. The initial system time was $t_0=-5$ ps and the maximum electric field amplitude [Eq. (4)] occurred at $t=0$ ps. As can be seen from the trajectory snapshots, the capsid structure does not respond until well after the light pulse has scattered from the capsid at around $t=5$ ps.

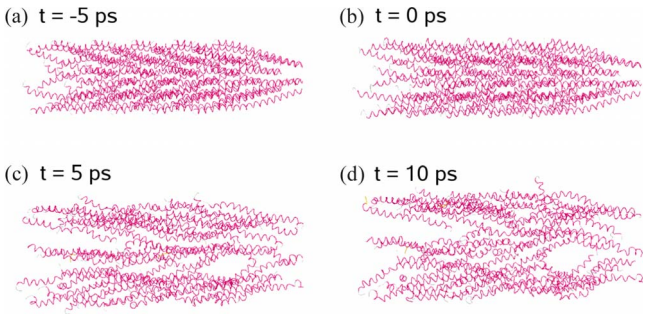

FIG. 6. (Color online) Four snapshot images of a 1 ns MD simulation of the unit cell of the M13 viral capsid for an incident pulse of duration $\tau_L=1$ ps and intensity 1.5 PW/cm^2. The peak of the Gaussian pulse occurs at $t=0$. The snapshots shown are for (a) $t=-5$ ps (before the pulse arrives), (b) $t=0$ ps (at the peak of the light pulse), (c) $t=5$ ps (shortly after the pulse), and (d) $t=10$ ps (significantly after the pulse). The intensity of the pulse is large enough to completely destroy the virus by $t=10$ ps.

It is possible that the capsid structure is only stable in the presence of its single stranded circular DNA. For example, a recent MD simulation by Freddolino *et al.* [23] of the satellite tobacco mosaic virus has shown that (at least in MD simulations) the capsid of the satellite tobacco mosaic virus is unstable without the RNA present. To make sure that the capsid was broken apart as a result of the impulsive scattering process and not from either a lack of genetic material or explicit water, we performed a 1 ns control simulation where the impulsive force was turned off. This simulation was performed in the canonical ensemble (constant temperature constant volume) at a temperature of 300 K. All other simulation details were the same as the MD simulations where the impulsive force was on. The results (not shown) clearly illustrate that the capsid is stable over at least 1 ns and that the capsid in Fig. 6 is indeed breaking apart as a result of the additional impulsive force from light.

It is clear when the viral capsid breaks apart but it is not clear from the images which conditions (laser intensity and pulse duration) produce minor damage to the capsid. To assess this we monitor various properties of the capsid as a function of time and under different conditions. The properties we monitor are (i) the (quasi)temperature rise of the capsid, (ii) the number of interprotein contacts (IPCs), and (iii) the solvent accessible surface area (SASA).

Our ISRS simulations always start at zero temperature. We use this limit to better determine the effects of just the laser pulse. It is certainly expected that more damage will occur to the virus at room temperature so that these simulations provide a lower bound for the damage.

Figure 7 shows the (quasi)temperature rise of the capsid due to the laser pulse. The temperature rise is defined through the additional kinetic energy (KE) imparted to the atoms of the capsid from the laser pulse, $\frac{3}{2}NkT=\Delta E_{\mathrm{KE}}$, where N is the total number of atoms. Thus the (quasi)temperature is a measure of the kinetic energy imparted to the capsid from the light scattering and not a true thermodynamic temperature. Two cases are shown; (a) shows the temperature rise for a 10 ps pulse, and (b) shows the temperature rise for a 0.10 ps pulse time. Each of these figures shows the result for multiple laser intensities. In Fig. 7(a) (10 ps) it is noted that the two lowest intensities do not cause the capsid to obviously break apart, yet the temperature rise does not show any key signature difference between those that do break apart and those that do not (see Table II). In contrast, we note that in Fig. 7(b) (0.10 ps) there is a clear difference between the temperature curves for intensities above and below 1.5 $\mathrm{PW/cm^2}$.

Next we consider the IPCs of the viral capsid. An IPC is defined as any pair of atoms within a distance range R_{IPC}, where each of the two atoms resides on a protein polypeptide strand on separate distinct proteins. The value of R_{IPC} chosen is 3 Å. The value is somewhat arbitrary but was meant to include salt-bridges, hydrogen-bonds, and close hydrophobic contacts. Figure 8 shows the number of IPCs for the M13 capsid as a function of time due to a laser pulse of duration (a) 10 ps and (b) 0.10 ps with several different laser intensities. For the longer pulse (a) of $\tau_L=10$ ps, there is an enormous drop in the IPC even at the peak of the pulse at $t=0$. There is a tendency to "heal" some of the damage for the lowest laser intensities. For the short pulse (b) of $\tau_L=0.10$ ps, there are clear signatures of damage long after the pulse. All capsids show a drop in IPCs long after the pulse has passed and at the highest intensities, only about $\frac{1}{2}$ of the initial IPCs remain. Note the curious feature near $t\approx 0$, at the peak of the pulse, the IPC number actually grows. This is indicates a compression of the capsid by the laser.

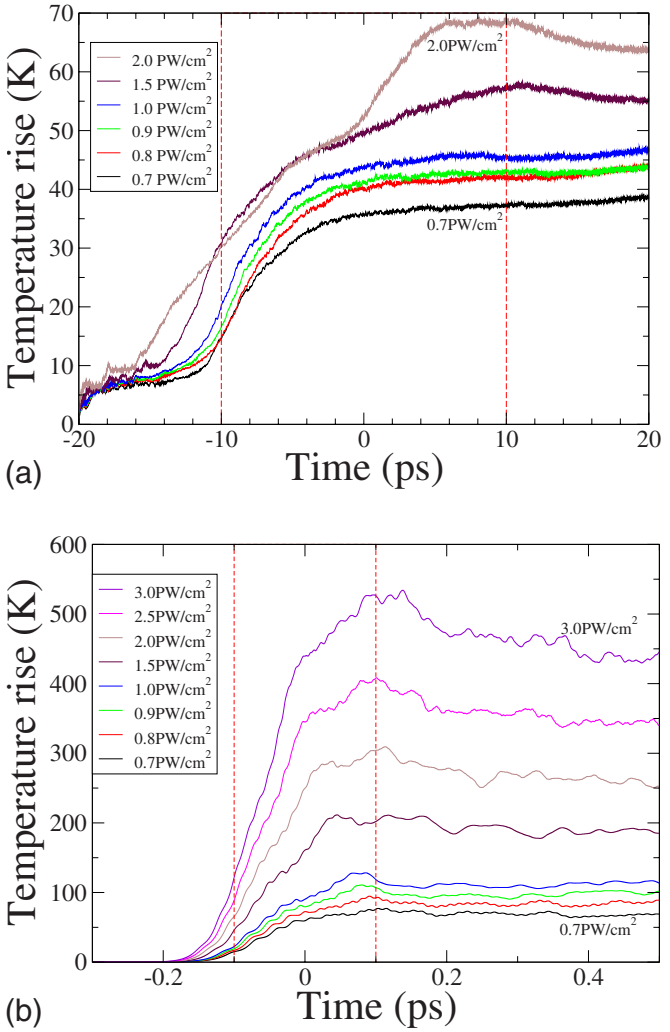

FIG. 7. (Color online) Temperature rise vs time for (a) a 10 ps pulse and (b) a 0.10 ps pulse. There is a clear separation in temperature between those intensities greater than 1 $\mathrm{PW/cm^2}$ and less than 1 $\mathrm{PW/cm^2}$ after the laser pulse is off. The vertical dashed lines represent the temporal region $\pm\tau_L$ of the pulse peak.

The SASA is another measure of disassembly of the viral capsid. The SASA is a measure of the accessibility of atoms (such as solvent) to the surface of the protein [24]. A compact protein or proteins in close contact with other protein have a small SASA. We use the method of Dictionary of Protein Secondary Structure (DSSP) [25] with a radius of water equal to 1.40 Å to measure the SASA as the protein undergoes dynamical changes due to the laser pulse. Figures 9(a) and 9(b) show the SASA for a pulse time of 10 ps and 0.1 ps for various intensities. In Fig. 9(a), the SASA before the pulse is near $0.9\times 10^{+5}$ Å and then grows to about $1.8\times 10^{+5}$ Å for the 1.5 $\mathrm{PW/cm^2}$, which breaks the capsid

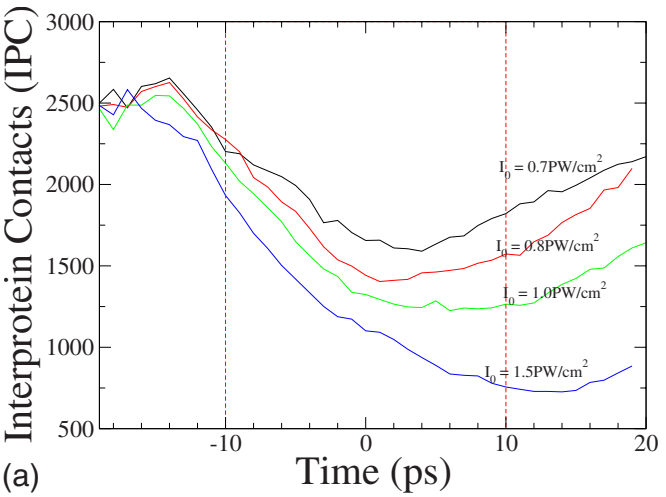

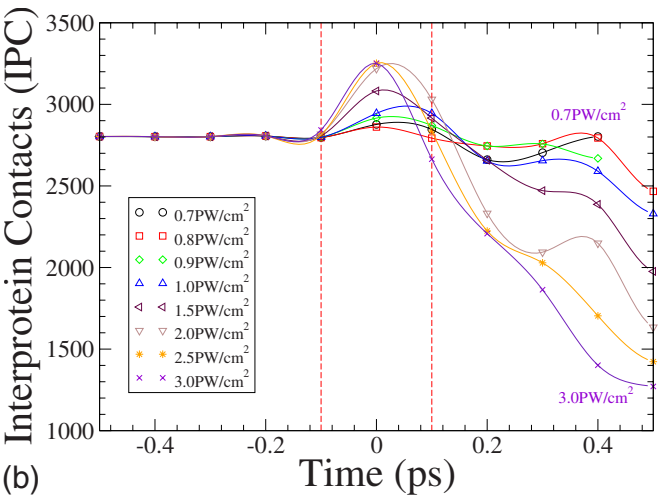

FIG. 8. (Color online) The number of interprotein contacts (IPCs) within a cutoff distance of $R_{\mathrm{IPC}}=3$ Å vs time for (a) a 10 ps pulse and (b) a 0.10 ps pulse. The vertical dashed lines represent the temporal region $\pm\tau_L$ of the pulse peak.

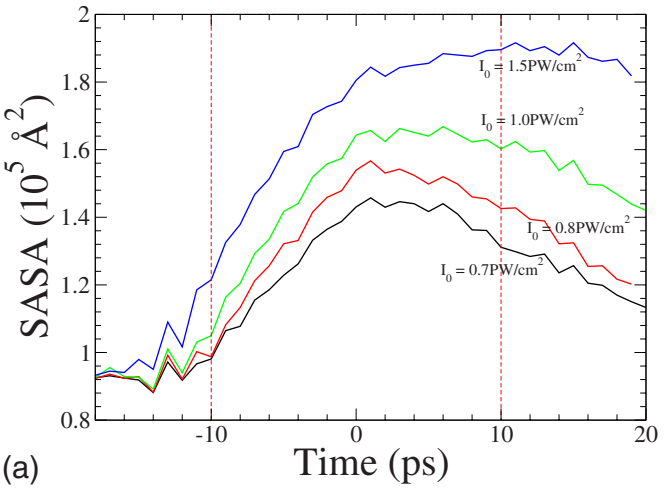

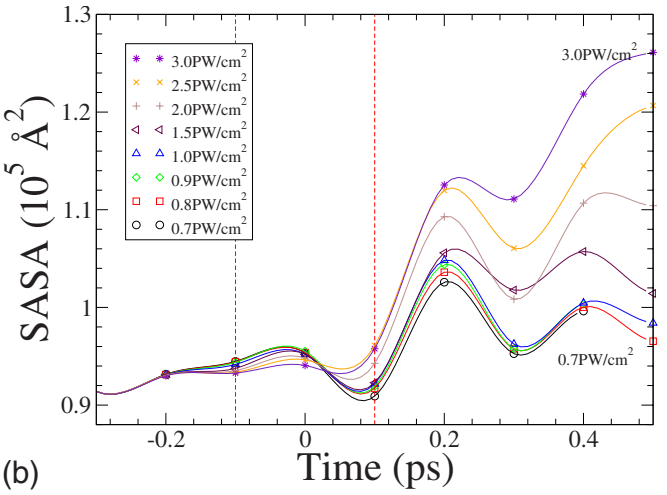

FIG. 9. (Color online) Solvent accessible surface area (SASA) vs time for (a) a 10 ps pulse and (b) a 0.10 ps pulse. The vertical dashed lines represent the temporal region $\pm\tau_L$ of the pulse peak.

apart. We note that for lower powers the capsid SASA expands to about $1.4\times10^{+5}$ Å, which is a 50% increase over its initial value. In Fig. 9(b) we see much the same type behavior as in Fig. 9(b) except that the four lowest intensities, which were seen to not break the capsid, maintain approximately the same SASA after the laser pulse is gone.

VIII. DISCUSSION

One would initially guess that capsid damage is simply dependent on the length of the laser pulse or on total energy delivered to the capsid. However, the pulse width plays a surprising role. In a simple driven harmonic oscillator description of the problem, the maximum amplitude of vibrational motion occurs for vibrational modes of the capsid which have a period that is roughly four times the pulse width τ_L. However, interprotein interactions are influenced most by low frequency modes of which there are few. There are an abundance of high frequency bond-stretching modes where excitation of them with the laser may be thought of as a heating of the capsid. The coupling between the high frequency reservoir of modes and the few low frequency modes due to anharmonicity and other mechanisms governs the energy exchange between these two reservoirs. Interestingly though, the TED data from Table I suggests that the severe M13 capsid damage seems to be independent of the total energy that is delivered to the capsid. This suggests that a single mode, or a minor few, is responsible for breaking apart the capsid.

A disturbing feature of our results is the very high intensities of light that were required in order damage the capsid. The experiments that have been performed use intensities of light [1–4] that are at most of order 10–100 $\mathrm{GW/cm^2}$ in intensity and even as low as 60 $\mathrm{MW/cm^2}$. Our simulations use an intensity of order 1 $\mathrm{PW/cm^2}$, which is of order 10^4 or larger. Thus our simulations indicate that a single laser pulse at the intensities used in the experiments produce no or very little damage through the ISRS mechanism alone.

The inactivation of viruses in experiments is found here not to be well explained by ISRS. Another potential mechanism is two-photon absorption. Although a single photon (say at 800nm) is below the absorption threshold within the

protein, the much weaker process of absorbing two photons could conceivably be above the absorption threshold. This could result in absorption within specific residues and produce athermal "hot spots" within the capsid. Research in this direction will be considered in future work. Here we obtain a simple estimate of the two-photon absorption in tryptophan, an often mentioned candidate for two-photon effects in proteins. The cross section of 3.2×10^{-52} cm^4 s [26] produces a probability of 6×10^{-7}/pulse of absorbing two photons in the presence of an incident light intensity of 100 $\mathrm{GW/cm}^2$. This too is a small effect. Additionally, the low energy single absorption tail of tryptophan occurs at about 300 nm, which for two-photon absorption requires a wavelength of about 600 nm for each photon. Yet near IR experiments of ultrashort laser pulses on the HIV pathogen [5] use light of 776nm and produce inactivation. Clearly, more work is necessary to determine the source of inactivation of viruses due to ultrafast laser pulses.

IX. CONCLUSION

We have presented a methodology to incorporate the impulsive force from an ultrashort pulsed laser on a molecule in a molecular-dynamics simulation. The method is based on an empirical bond-polarizability model and can be used for the modeling of interactions of media with *short* light pulses. The impulsive force equations derived in this article were used in a molecular-dynamics study of the M13 bacteriophage capsid and compared with a simple driven harmonic oscillator to develop a basic qualitative understanding of the physics involved with impulsive Raman scattering of viral capsids. The MD results show that an M13 capsid is damaged for rather large intensities. The damage seen in experimental studies [3] occurs at far lower thresholds. The ISRS mechanism from a single laser pulse does not explain the clear damage seen in experiments with ultrashort laser pulses.

[1] K.-T. Tsen, S.-W. Tsen, T.-C. W. C. L. Chang, C.-F. Hung, T.-C. Wu, and J. Kiang, Virol. J. **4**, 50 (2007).
[2] K.-T. Tsen, S.-W. Tsen, O. F. Sankey, and J. Kiang, J. Phys.: Condens. Matter **19**, 472201 (2007).
[3] K.-T. Tsen, S.-W. Tsen, C.-L. Chang, C.-F. Hung, T.-C. Wu, and J. G. Kiang, J. Phys.: Condens. Matter **19**, 322102 (2007).
[4] K.-T. Tsen, S.-W. Tsen, C.-L. Chang, C.-F. Hung, T.-C. Wu, and J. G. Kiang, J. Biomed. Opt. **12**, 064030 (2007).
[5] K.-T. Tsen, S.-W. D. Tsen, C.-F. Hung, T.-C. Wu, and J. G. Kiang, J. Phys.: Condens. Matter **20**, 252205 (2008).
[6] B. Stephanidis, S. Adichtchev, P. Gouet, A. McPherson, and A. Mermet, Biophys. J. **93**, 1354 (2007).
[7] K. T. Tsen, E. Dykeman, O. Sankey, S.-W. D. Tsen, N.-T. Lin, and J. Kiang, Nanotechnology **17**, 5474 (2006).
[8] N. J. English and D. A. Mooney, J. Chem. Phys. **126**, 091105 (2007).
[9] Y.-X. Yan, E. B. Gambel, and K. A. Nelson, J. Chem. Phys. **83**, 5391 (1985).
[10] S. Go, H. Bilz, and M. Cardona, Phys. Rev. Lett. **34**, 580 (1975).
[11] D. Bermejo, S. Montero, M. Cardona, and A. Muramatsu, Solid State Commun. **42**, 153 (1982).
[12] S. Guha, J. Menéndez, J. B. Page, and G. B. Adams, Phys. Rev. B **53**, 13106 (1996).
[13] D. W. Snoke and M. Cardona, Solid State Commun. **87**, 121 (1993).
[14] E. C. Dykeman, O. F. Sankey, and K.-T. Tsen, Phys. Rev. E **76**, 011906 (2007).
[15] E. C. Dykeman and O. F. Sankey, Phys. Rev. Lett. **100**, 028101 (2008).
[16] D. A. Marvin, L. C. Welsh, M. F. Symmons, W. R. P. Scott, and S. K. Strauss, J. Mol. Biol. **355**, 294 (2006).
[17] N. W. Ashcroft and N. D. Mermin, *Solid State Physics*, 2nd ed. (Saunders College, Philadelphia, 1976).
[18] W. D. Cornell, P. Cieplak, C. I. Bayly, I. R. Gouldand, K. M. Merz, D. M. Ferguson, D. C. Spellmeyer, T. Fox, J. W. Caldwell, and P. A. Kollman, J. Am. Chem. Soc. **117**, 5179 (1995).
[19] V. Tsui and D. Case, Biopolymers **56**, 275 (2001).
[20] D. Bashford and D. Case, Annu. Rev. Phys. Chem. **51**, 129 (2000).
[21] G. D. Hawkins, C. J. Cramer, and D. G. Truhlar, J. Phys. Chem. **100**, 19824 (1996).
[22] E. Dykeman and O. Sankey, J. Phys.: Condens. Matter **21**, 035116 (2009).
[23] P. L. Freddolino, A. S. Arkhipov, S. B. Larson, A. McPherson, and K. Schulten, Structure **14**, 437 (2006).
[24] B. Lee and F. Richards, J. Mol. Biol. **55**, 379 (1971).
[25] W. Kabsch and C. Sander, Biopolymers **22**, 2577 (1983).
[26] P. Sengupta, J. Balaji, R. Philip, G. R. Kumar, and S. Maiti, Proc. SPIE **4262**, 336 (2001).